INTEGRAL

Science Operations Centre

Announcement of Opportunity for Observing Proposals (AO-7)

SPI Observer's Manual

INT/OAG/08-0295/Dc

Issue 1.0

12 January 2009

Prepared by C. Sánchez-Fernández

Authorised by A. N. Parmar

Based on inputs from:

J.P. Roques, SPI Co-PI, CESR Toulouse

R. Diehl, SPI co-PI, MPE Germany

Table of Contents

1 Introduction

The SPectrometer onboard INTEGRAL (SPI) is one of the two prime instruments of the INTEGRAL scientific payload. SPI is a high spectral resolution gamma-ray telescope devoted to the sky observation in the 20 keV - 8 MeV energy range, using an array of 19 closely packed germanium detectors. SPI instrument is the first high resolution gamma ray spectral imager to operate in this energy range. The spectral resolution is fine enough to resolve astrophysical lines and allow spectroscopy in the regime of gamma-rays. The coded mask provides imaging at moderate resolution. The main characteristics of the instrument are given in Table 1. An overall cut-view of the instrument is shown in Figure 1.

Table 1- Main characteristics of the SPI instrument.

Detector dimensions	60 mm wide surface, 70 mm deep
Mask dimensions	665 mm flat to flat 30 mm thick Tungsten
Detector unit	Encapsulated Ge, hexagonal geometry, 19 detectors 70 mm thick
Energy range	20 keV - 8 MeV
Energy resolution (FWHM)	2.2 keV at 1.33 MeV for each detector, 3 keV for the whole spectrometer.
Angular resolution	2.5^o for point sources
Point source positioning	$<1.3^o$ for point sources (depending on point source intensity)
Field-of-View	fully coded: 14^o flat to flat, 16^o corner to corner zero coding: 32^o flat to flat, 35^o corner to corner (zero sensitivity)

Science objectives of SPI are nucleosynthesis, relativistic-particle accelerators, and strong-field signatures in compact stars; this is studied through nuclear lines and spectral features in accreting binaries, pulsars, or solar flares, but also through energetic continuum radiation in the 20keV- 8MeV range from the variety of cosmic sources, including active galactic nuclei and gamma-ray bursts.

SPI is a collaborative international project developed for ESA under the responsibility of CNES Toulouse (France) as prime contractor. Subsystems for SPI have been built by: LDR and MPE (Germany; Anti-coincidence subsystem), the University of Louvain (Belgium; Germanium for detectors), CESR (France; Ge detectors and their electronics), CEA-Saclay (France; Digital Front End Electronics), CNES (France; cryostat, lower structure, flight software, thermal control), University of Valencia (Spain; coded mask), IFCTR Milano (Italy; Plastic Scintillator)

and the University of Berkeley and San Diego (USA; Pulse Shape Discriminator). The two Co-PIs responsible for the SPI instrument are J.P. Roques (CESR, Toulouse, France) and R. Diehl (MPE, Garching, Germany).

The following sections provide a description of the instrument (Section 2), its operations (Section 3), its performance (Section 4) and some hints on the use of the instrument (Section 5; "cook book"). For further details we refer the interested reader to a series of papers on the SPI instrument in the A&A special INTEGRAL issue (2003, vol 411, L63-L113). This issue also contains various other papers on the first results from in-flight observations. For a description of the SPI data analysis, we refer also to the special INTEGRAL issue (2003, vol 411, L117-L127) and the SPI validation report of the Off-line-Scientific Analysis (OSA) software package released by the ISDC. Besides, the descriptions of the data analysis pipelines and modules and the use of the OSA software can be found at the ISDC website (http://isdc.unige.ch/?Soft+download).

2 Description of the instrument

2.1 Overall design

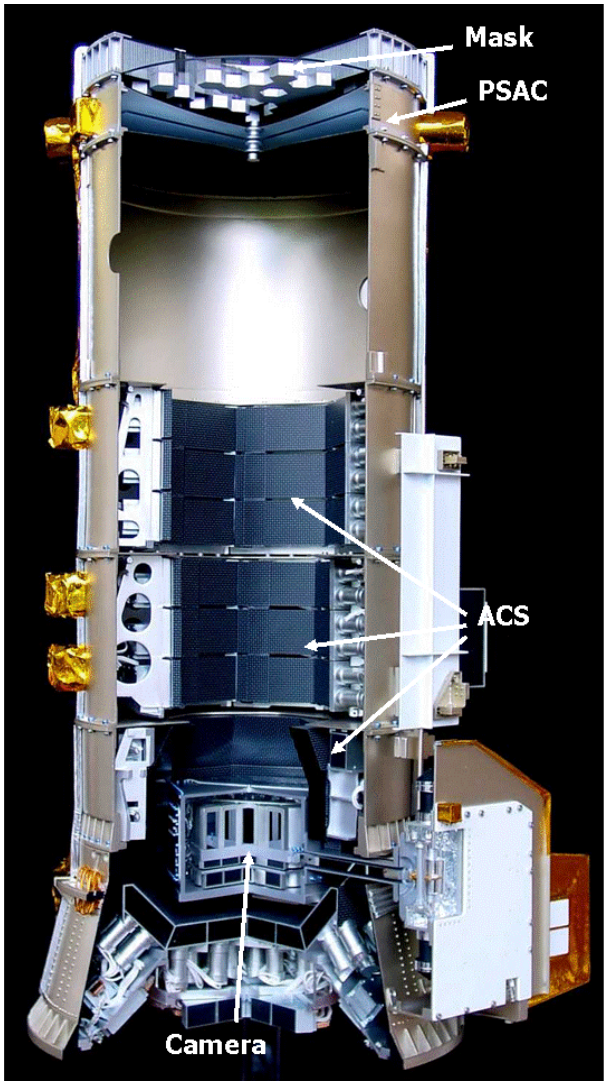

Figure 1 - A cut-away view of the SPI instrument.

SPI is a coded mask spectrometer, composed of the following main subsystems:

- the camera, with 19 cooled, hexagonally shaped, high purity germanium detectors (GeDs) and their associated electronics;

- a two-stage cooling system, composed of a passive stage and an active stage;

- a pulse shape discrimination system (PSD) which allows discrimination between single and multi-site interactions in one Ge detector;

- an active anti-coincidence shield (ACS) made of 91 BGO blocks;

- a plastic scintillator (PSAC), to limit the background on the detector; the electronics, providing the SPI internal timing, the various (anti)coincidence functions and the primary data encoding;

- a coded mask, which allows imaging of the sky.

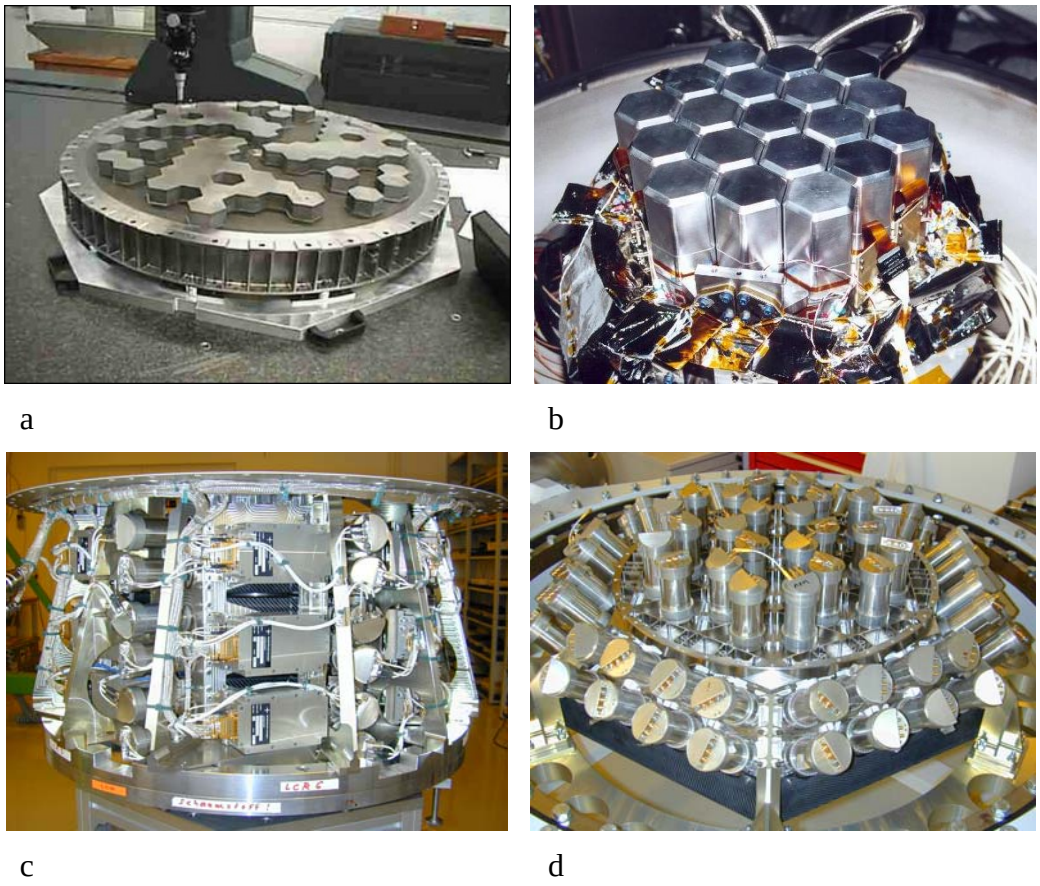

a b c d

Figure 2 - View of some subsystems of the spectrometer: a) coded mask; b) detector plane; c) lower collimator ring, side view; d) rearshield assembly.

In the following subsections we describe briefly these subsystems. For the interested reader, a more detailed description of SPI can be found in Vedrenne et al. (2003, A&A vol 411 L63).

2.1.1 Detectors and pre-amplifiers

The detectors used for SPI are 19 reverse-electrode n-type Ge detectors (GeDs). They have an hexagonal shape with a size of 5.6 cm, flat to flat, and a height of 69.42 mm. The GeDs are mounted with minimum space between them, such that the axes of two adjacent detectors are 6 cm apart. Each crystal is mounted in an Al capsule.

The hexagonal shape was chosen to minimize the volume occupied by the detector array, and therefore the volume and the weight of the anti-coincidence system, which surrounds the camera (see 2.4). To reduce the leakage current and to slow the effects of radiation damage, high purity germanium detectors have to be operated at cryogenic temperatures. Therefore, the closely packed array of GeDs is fixed on a (cold) Beryllium plate, and the detector array is placed inside

a cryostat (see 2.2.3). The bottom side of the cold plate houses the first stage of the preamplifier circuitry (PA-1), which has only passive components. The PA-1 electronics include the high voltage filter and the connection between the detector and the Charge Sensitive Amplifier (CSA). A second set of 19 pre-amplifiers (PA-2) is mounted on a second cold plate established at 210 K and thermally connected to the cryostat. This stage includes the FET, for which the low temperature allows a reduction of the electronic noise.

Currently, only 17 out of the 19 detectors are operated, following failures of detectors #2 in December 2003 and #17 in July 2004.

2.1.2 The detector electronics

The signals from the pre-amplifiers are sent to the amplification chain, which is made up of a Pulse Shape Amplifier (PSA) and a Pulse Height Amplifier (PHA). The PSA amplifies the pulses such that the performance of the spectrometer is optimised. The PSA also provides a timing signal used for time-tagging each analysed event. The pulse heights are coded by the Pulse Height Analyser (PHA; 16384 channels in two energy ranges: 0-2 MeV and 2-8 MeV). For the first energy range, each channel has a resolution of 0.13 keV, while for the second range, one channel corresponds to 0.52 keV.

The detector electronics also comprise a high voltage power supply (0-5000 V) for the Ge detectors and a low voltage power supply for the pre-amplifiers (19 independent chains per amplification chain).

2.1.3 Cryostat

For an optimum sensitivity and resolution, the Ge detectors must be kept at a constant cryogenic temperature. The SPI cryostat is designed to keep the detectors at the operating temperature. It also provides the functions necessary for Ge crystal annealing. The cryostat is composed of three systems: an active cooling system, a passive cooling system and a cold box.

The active cooling system brings the temperature of the cold plate, on which the detectors are mounted, down to 80 K. The cooling is obtained by 4 mechanical Stirling cycle coolers. The performance of the mechanical coolers in terms of heat lift is limited to a few Watts, so the Ge detectors have to be very well thermally insulated from their environment. Therefore, the detection plane is enclosed in a beryllium structure (cold box) controlled at an intermediate temperature (210 K) through a passive cooling device.

All temperatures of the cryostat subsystems are regularly monitored to provide the ground operators with early warnings in case of failures of the coolers, and to provide temperature information that can be used for the data processing.

2.2 Pulse Shape Discriminator (PSD)

The PSD subsystem compares the shape of the pulses produced by the pre-amplifiers, with profiles stored in an onboard archive. It was aimed at reduction of β-decay background in the Ge detectors. Experience obtained during the early mission revealed that using the information from the PSD does not significantly increase the signal to noise ratio: it is therefore currently not used.

2.3 Anti-Coincidence Subassembly (ACS)

The main function of the Anti-Coincidence Subassembly (ACS) is to shield the Ge detectors against background (photons and particles) from sources outside the field-of-view. The SPI ACS consists of 91 bismuth-germanate (BGO) scintillator blocks arranged in 4 subunits: two collimator rings (the upper and lower collimator ring, located between the coded mask and the detector plane) whose axes are along the viewing direction of the spectrometer; the side-shield and the rear-shield assemblies, that surround the camera. The BGO crystal thickness was optimised via Monte Carlo simulations to minimize the detector background, because a too high mass of BGO can increase secondary neutron production, producing extra background in the Ge crystals.

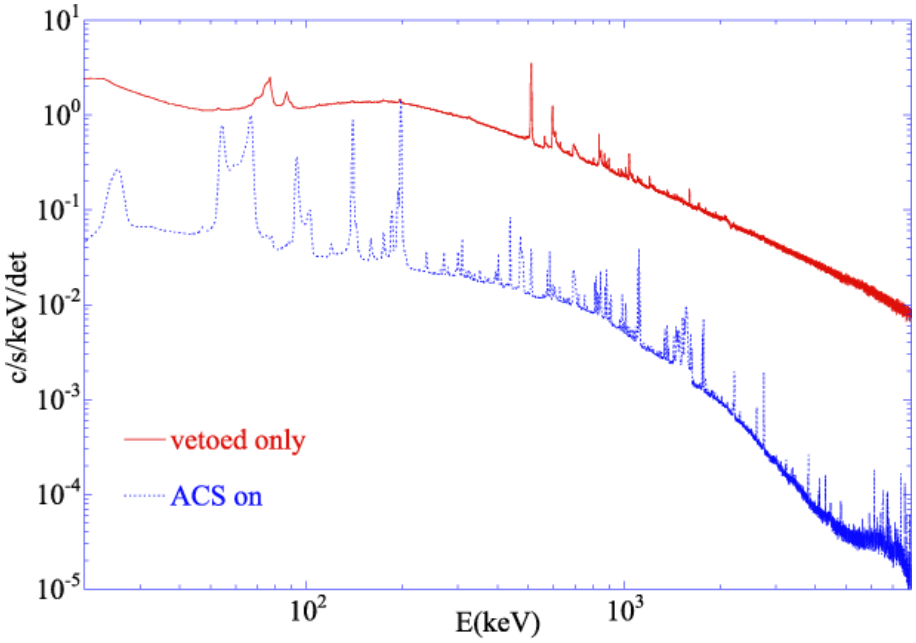

Figure 3 – SPI background spectra of GeD events in anticoincidence with an event in the ACS ("ACS on") and in coincidence with an event in the ACS ("vetoed only"). The total rate in the 20 keV-8000 keV range changes by a factor of ~25 between both configurations (Jean et al. 2003, A&A vol. 411, L107).

The BGO scintillator crystals convert all incoming events into photons in the 480 nm region (visible light). Photo-multiplier tubes are then used to detect these photons and convert them into electrical pulses, which are combined into an overall veto signal. The ACS output data is directed to the Digital Front End Electronics (DFEE, see Sect. 2.6). The latter formats the data, and time-tags each event. Photons that are not in coincidence with an ACS veto event are considered as “good”. Additionally, the DFEE time-tag these events, and transmit event rates at a 50 ms resolution. These can be used, e.g., for Gamma-Ray Burst (GRB) studies (see Sect 3.8 for detailed information on GRB detection by SPI/ACS). Photons that occur outside the ACS veto signal are considered, sorted, normalised and summed up by the ACS electronics.

The ACS significantly reduces the instrument background as can be seen in Figure 4, which shows background spectra of the GeD events that did not coincide ("ACS on") or that did coincide ("vetoed only") with a trigger of the ACS. The total rate (in the 20 keV-8000 keV range) changes by a factor of ~25 between both configurations.

2.4 The Plastic Scintillator Anti Coincidence Subassembly (PSAC)

The purpose of the Plastic Scintillator Anti-Coincidence Subassembly (PSAC) is to reduce the 511 keV background due to particle emission by the passive mask. The PSAC consists of a plastic scintillator inside a light tight box, located just below the passive mask. It has a good gamma-ray transparency, and actively detects particles which deposit energies in excess of 300 keV. The light flashes produced by the impacts of high energy particles on the scintillator are detected with two photo-multiplier tubes located around the light-tight box and converted into electrical pulses. They are processed by the PSAC electronics assembly, which then sends to the DFEE a signal associated with the detected events, and compatible with the ACS veto signal. In-flight calibrations have shown that the PSAC provides background reductions of the order of a few %.

2.5 Electronics

The SPI electronics is divided into the Digital Front End Electronics (DFEE) and the Data Processing Electronics (DPE). The DFEE are in charge of the real-time acquisition, assembly, time-tagging and synchronization of the various signals from the SPI front end (detector electronics, PSD, ACS, etc). The DFEE subdivide the events into classes depending on their origin in the instrument and handle overall event energies and system monitoring statistics (dead time, signal counts, etc). Detected events are time-tagged with a 20 MHz local clock, which provides the timing resolution. The reset (timing reference) is done with the 8 Hz satellite clock. The statistics are passed on to the DPE every second. The DPE are part of the On-Board Data Handling (OBDH) unit. It provides the telecommand and telemetry interfaces to the instrument and the environment for the instrument dedicated software (Instrument Application Software, IASW).

2.6 The passive mask

The imaging capability of the spectrometer is obtained with the help of a coded-aperture mask, which codes the incident gamma rays in the field-of-view. The passive mask is located at the top of the instrument, above the plastic scintillator, and 171 cm from the detector plane. The distance is driven by the required field-of-view and angular resolution. The mask also provides stiffness to the primary structure of SPI.

The mask has a sandwich structure made of a nomex honeycomb core covered by two skins, a titanium ring that forms the interface to the rest of the instrument, and a coded motif made of 127 hexagonal elements. 63 of these elements are made of 3 cm thick tungsten and are opaque to gamma-ray radiation within the SPI operational range, with an absorption efficiency >95% at 1 MeV. The other 64 elements are nearly free of matter, and thus almost transparent to gamma-rays: they have a gamma-ray transparency of 60% at 20 keV and 80% at 50 keV. The imaging principle of a mask is based on the fact that each gamma-ray source in the field of view throws a shadow on the detector. Since the “shadowgrams” of different sources are independent from

each other, a deconvolution technique allows the reconstruction of sky-maps, with resolved source positions.

The mask-detector arrangement defines a fully-coded field of view of 16^o x14^o (y/z dimension) and partially-coded field of view of 26^o x 23^o respectively. An image of the mask pattern is provided in Figure 2.

3 Instrument operations

3.1 How the instrument works?

The operating mode of SPI is based on the detection of GeD events which are in the 20 keV-8 MeV tenergy range, and which are not accompanied by ACS events. The events can be single detector events (SE), with photon energy deposit in only one detector, or multiple detector events (ME), which arise from an interaction cascade of a single primary photon with energy deposits in more than one detector. In this case, the sum of the energy deposits corresponds to the total energy deposited by the initial photon. All events are processed by the DFEE, which provides event timing with 102.4 μs accuracy, event building and classification, and event rejection, using the ACS veto signal. The events are also counted and the dead time is permanently monitored. The DPE receive from the DFEE all the data, assemble all the information, and send the resulting stream to the satellite telemetry downlink system.

SPI provides a combination of high-resolution spectroscopy with imaging capabilities. The performance characteristics of the instrument depend on the instrumental design as follows:

- Energy resolution: it is determined by the cooled Ge detectors.
- Angular resolution: it is determined by the pixel size of both the mask and the detector, and by the distance between them. Since the GeD assembly consists of only 17 detectors, an image of the sky is not unambiguously defined by the “shadowgram” pattern. The ambiguity is resolved by introducing dithering steps of the telescope axis, around the direction of the gamma-ray source to be studied (dithering).
- Field-of-view: it is defined by the area of the mask, the germanium detector assembly, the distance between them, as well as the ACS shield.
- Narrow line sensitivity: achieved by making the detector as large as possible, by minimizing the background (using an ACS optimised in material and thickness), by choosing carefully the materials used in the instrument, and by adding a PSAC below the mask.
- Timing accuracy: requires a high telemetry rate, because the events are recorded photon-by-photon.

3.2 SPI operating modes

SPI has only one mode for normal observations, the so-called “photon by photon” mode, which has a high time resolution. In this mode, scientific data are collected and transmitted to the ground for each detected (non-vetoed) photon, from which the type of event, the energy and the timing can be deduced. Furthermore, detector spectra of all events (including vetoed ones) can be accumulated and transmitted every 30-60 minutes.

In case the SPI telemetry is continuously overflowing due to background radiation higher than expected, or due to a strong solar flare, the instrument can be operated in a “degraded” science mode (TM emergency mode). In this case, the on-board processing and transmission of data will be restricted to “good” events (non-vetoed). The maximum data generation rate in this mode

will be about half the rate for normal photon by photon mode. The observer cannot select the TM emergency mode: in case it is needed, ground controllers command it.

Before any change of mode, the SPI instrument will be put into a special configuration mode. This is the only mode in which changes to the instrument configuration can be made. SPI will not be taking scientific data when in configuration mode (science telemetry processing is stopped). Several other special modes are available for engineering tasks (e.g., annealing) and for instrument calibrations; they are not of interest to the general observer.

3.3 Dead time

Due to several causes (e.g., veto signals), SPI experiences, within a normal exposure, a dead time during which no useful scientific data are collected. It depends on several external conditions (e.g., increase of the ACS rate during a solar flare). Experience obtained during previous AOs has shown that the dead time is about 15% of the observing time.

3.4 Telemetry budget

INTEGRAL uses packet telemetry (TM). Each packet corresponds to 0.44 kbps. For SPI, the background mainly determines the telemetry usage. The telemetry allocated to SPI was changed several times since the launch of INTEGRAL to be adapted to the real background, and to follow its evolution (for example, it depends on the solar activity). Since May 2006, the TM allocation for SPI is 105 packets per cycle.

3.5 Spectroscopy

In the standard observing mode, the instrument can be used for spectroscopic observations. In the energy range of SPI, the signal-to-background ratio is in general small (typically a few to 10%). Knowing the background is critical to produce high quality gamma-ray spectra. Furthermore, the background in each of the 19 (17 currently operational now) independent detectors can vary in time in a different way, further limiting the instrument sensitivity. To solve the uncertainties in the background determination, an appropriate dithering strategy has to be adopted for every observation (see the *"Mission Overview Policies and Procedures"* document for further details). Dithering is also important to improve the image quality of the reconstructed sky images (see 3.7). Therefore, *all SPI observations should use dithering, since background calculation for staring observations is very difficult, if not impossible, due to background in-homogeneities over the detector plane*. The dithering strategy to be adopted depends on the characteristics of the field.

- Observations of a region with multiple or complex sources, or with sources which position is poorly known: the 5 x 5 rectangular dithering pattern should be used.
- Observations of a single point source of known location, where there are no other known objects of significant intensity in the field-of-view (fully and partially coded, for all dithering points, i.e., within a radius of about 20^{o}). In this case the hexagonal dithering pattern can be used. Note, however, that the number of sources for which this pattern can be used is very limited, and a justification in the proposal for this mode is required. Usually, only if SPI is not the main instrument, or when observing a single strong emission line, an hexagonal pattern can be justified.

3.6 Timing

In the standard observing mode (photon by photon) SPI can be used for timing analysis. Each photon data set includes timing information given by a 102.4 μs clock signal. This clock is synchronised to the on-board clock, and thus to the UTC, allowing for the instrument timing capabilities.

3.7 Imaging

In the photon by photon mode, the (x,y) coordinates of each event detected are registered and a "shadowgram" (i.e., a detector-plane image of the coded-mask shadow) is constructed. The sky image results from the deconvolution of the shadowgram, and the pattern of the mask. The imaging performance of SPI depends on the dithering pattern used: in general, the larger the number of pointings executed, the better the image reconstruction is.

Users must be aware that, when using the hexagonal dither pattern, the reconstructed point source response function shows very strong side lobes at distances of 10^o to 20^o from the centre. Therefore, this mode should only be used for isolated point sources and it is not really suitable for imaging. Experience obtained during previous AO's has revealed that there are not many isolated point sources (sometimes due to, e.g., transients) and observers are in general discouraged to use this mode. The side lobes are still present, but significantly less with the 5 by 5 dither pattern (about 50% of the hexagonal case). To remove these side lobes, which will cause artefacts in the reconstructed sky images, the only possibility is to enlarge the imaged area by observing with multiple pointings (i.e., multiple dither patterns).

3.8 Gamma-ray burst detection

One important contribution of the ACS to the science obtained with SPI is its use as a GRB monitor. The ACS shield provides a large effective area for the detection of bursts, Unfortunately, the electronics impedes spatial resolution of the detection, because only the total event rate of all crystals with 50 ms time resolution is sent down to Earth through TM packets. Therefore, accurate positions of gamma ray bursts that are detected with the ACS have to be determined through triangulation methods, with other (distant) spacecrafts. The INTEGRAL Science Data Centre (ISDC) software checks the stream of veto count rates automatically. If a gamma ray burst is detected (sudden increase in the count rate over a short period of time), an alert is issued to the 3rd Interplanetary Network (IPN) of gamma-ray bursts detectors. From the accurate timing of the SPI detection and detections by other spacecraft, a position is constructed and communicated to the scientific community. The accuracy that can be achieved with this method is much better than the arcminute (due to the long baseline, and the accurate timing of the SPI ACS events). The SPI-ACS data do not include spectral information because the energy of the interacting gamma-ray photons is not measured.

The ACS events are written to the instrument Housekeeping and are therefore made public immediately. Observers can be notified of these GRB events by subscribing to the INTEGRAL gamma-ray Burst Alert System (IBAS) of the ISDC: http://isdc.unige.ch/index.cgi?Soft+ibas. Information on the SPI/ACS triggers since the start of the mission is available from this URL, and also from the following MPE web page:

http://www.mpe.mpg.de/gamma/instruments/integral/spi/acs/grb/alerts.html.

The ACS detects a rate of 0.3 true GRB per day (minimal detectable energy flux between 4 and $7x10^{-7}$ erg $cm^{-2}s^{-1}$). In total, over 400 candidate GRBs have been detected since the INTEGRAL launch. Cosmic origin was confirmed for more than 50% of them (see, for example, Rau et al. 2005, A&A, vol. 438, 1175).

Note that GRBs can also be detected in the SPI field-of-view using the normal photon-by-photon mode. In this case, the GRB data rights belong to the observer who has an accepted proposal for GRBs in the FOV (see the document *"Mission Overview, Policies and Procedures"* for further details). A GRB in the SPI/IBIS field-of-view occurs about once per month.

4 Performance of the instrument

4.1 Components and sources of the SPI instrumental background

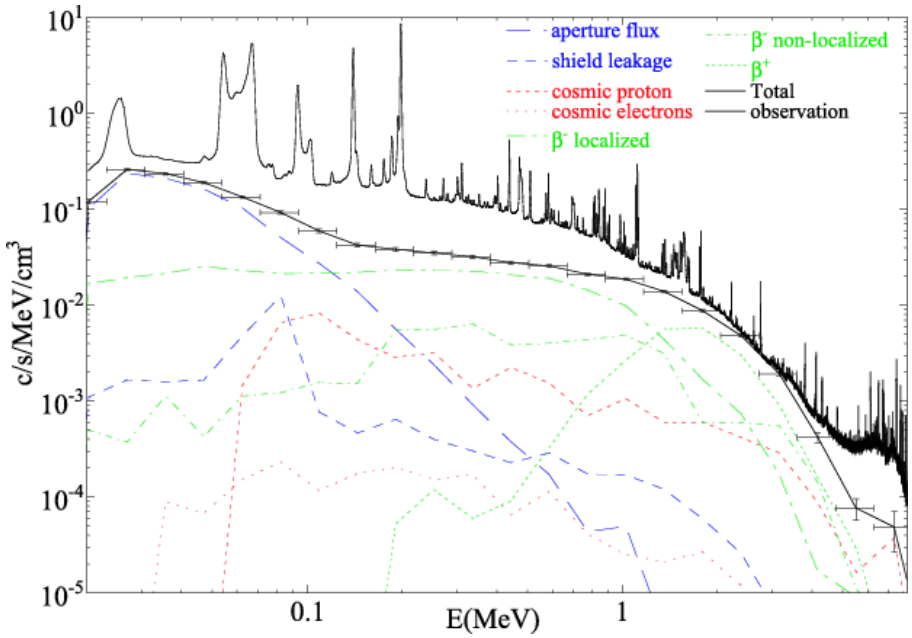

Figure 5 - Comparison of continuum background spectrum, estimated by simulation before the launch of INTEGRAL, with in flight background measurements. Different background components are also shown (Jean et al., 2003, A&A vol. 411, L107).

The sensitivity of instruments working in the high energy domain is mainly limited by the instrumental background. This is specially true for SPI, because it operates in an orbit outside the geomagnetic shield. Therefore, it is fully exposed to cosmic rays, which lead through nuclear-interaction processes with the instrument materials to a high background of false events.

The detailed physical processes involved are numerous and complex, but they can be simplified as follows: the incident cosmic radiation interacts, via inelastic collisions, with the detector nuclei, generating high energy secondary particles (like p, n, π^0, π^+…) and photons. The resulting protons and neutrons can produce, by nuclear interactions in the materials, radioactive isotopes. The subsequently decays, with a delay depending on their lifetimes, emit β particles and de-excitation photons. The β particles deposit their energies by Bremsstrahlung and generate a continuum energy distribution in the event spectrum. The de-excitation photons produce gamma-ray lines if they are totally absorbed in a single GeD, or undergo Compton scatterings, or pair production processes, and deposit only a part of their energy in the detector where the first interaction took place. The remainder energy can be deposited in one or even more of the neighbouring detectors. The number of multi-hit events increases drastically with energy.

In addition to these genuine gamma-ray events, there are other background events created in the detector via elastic neutron scatterings, which can only partially be recognized as background events.

The SPI background spectrum measured in flight is shown in Figure 6, which also plots the contribution of the various processes to the continuum. For further information on the SPI instrumental background and its variations, we refer the reader to Jean et al. (2003, A&A vol. 411 L107); for information on the identification and modelling of the SPI background lines, (see Weidenspointner et al. 2003, A&A vol. 411 L113 and references therein).

4.2 Measured performance

4.2.1 Imaging resolution

The SPI imaging performance is highly dependent upon the analysis method, the complexity of the field observed (in terms of number of sources, their flux stability, and their relative intensity) and the background handling. Note, however, that although the background is not uniformly distributed on the camera, its shape, determined from empty field observations for each energy bin, is relatively stable (Roques et al., 2003 A&A vol. 411, L91). The imaging capabilities of SPI are illustrated in Figure 5 (see also Bouchet et al., 2008, ApJ vol. 679, 1315 for results on deeper exposures).

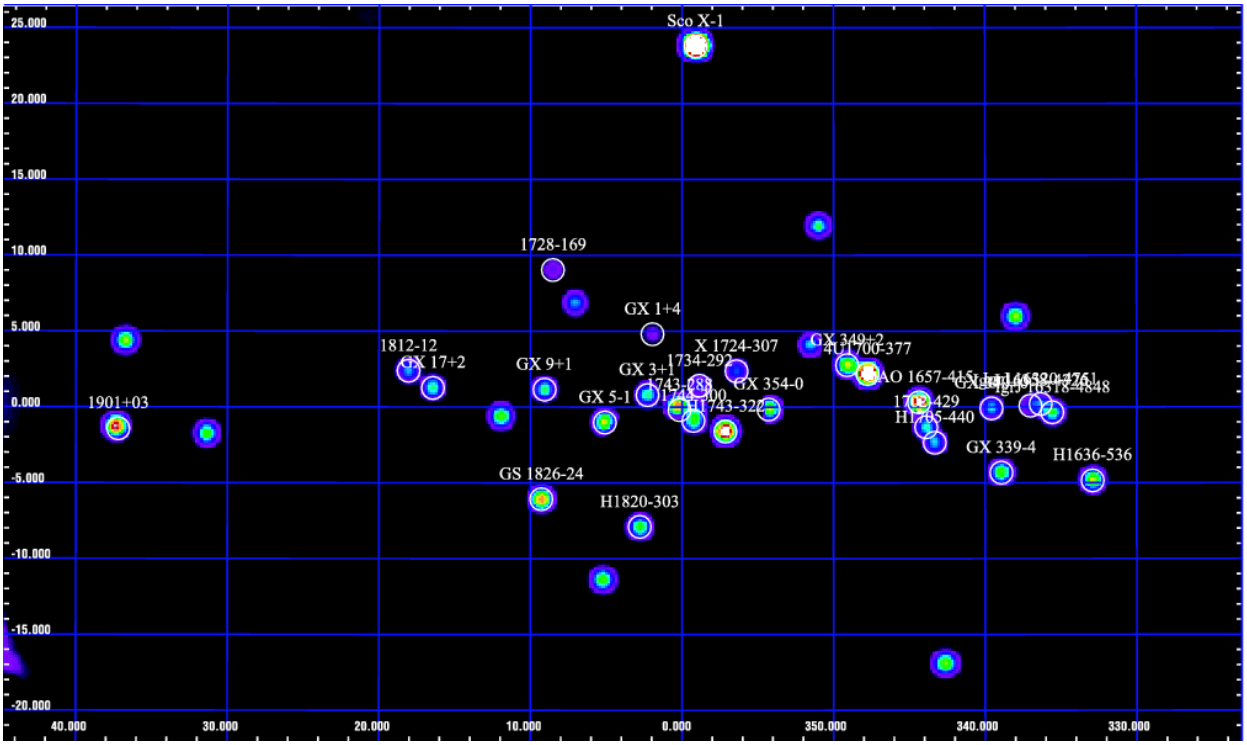

Figure 7 - The Galactic plane as observed by SPI during the Galactic Center Deep Exposure (GCDE) observation. Energy range: 20-50 keV (Roques et al., 2003, A&A vol. 411, L113)

The measured angular resolution for (isolated) point sources is about 2.5° (FWHM). This is the width of the instrument response correlation for a point source. Point sources can be located with better accuracy, but this depends on the strength of the source (the significance over the background) and locations of nearby sources. Strong sources can be located to an accuracy of 0.5 arcminute, while sources closer than 2 degrees will not be discriminated though imaging (see Dubath et al. 2005, MNRAS, 357, 420).

Positions measured by SPI have an uncertainty that is mainly statistical, and therefore count rate dependent. The uncertainties decrease as the inverse of the detection significance, and range from ~10 to ~1 arcminute for detection significances of ~10 to ~100. For higher detection significances (e.g., the Crab), the detection is ultimately limited to ~0.5 arcminute in position.

4.2.2 Energy resolution

The energy resolution of SPI was measured in the laboratory during pre-flight tests, with detectors representative of the flight units, and with flight model detectors plus pre-amplifiers. After launch, spectral resolution is monitored on a per-orbit and per-detector basis. This was found to be sufficient to yield an absolute accuracy better than 0.25 keV, and even better than 0.05 keV over a larger energy range (see for example Lonjou et al., 2004, ESASP vol. 552, L713). A spectrum measured in-flight, during a solar flare, is shown in Figure 8 to illustrate the capability of SPI to revolve lines in the MeV domain. The measured energy resolution for an individual detector is shown in Figure 9, and the energy resolution for the full instrument is given in Table 2. Observers should be aware that in regimes of strong instrumental lines (such as the 511 keV line), sensitivities are significantly worse than in between such lines.

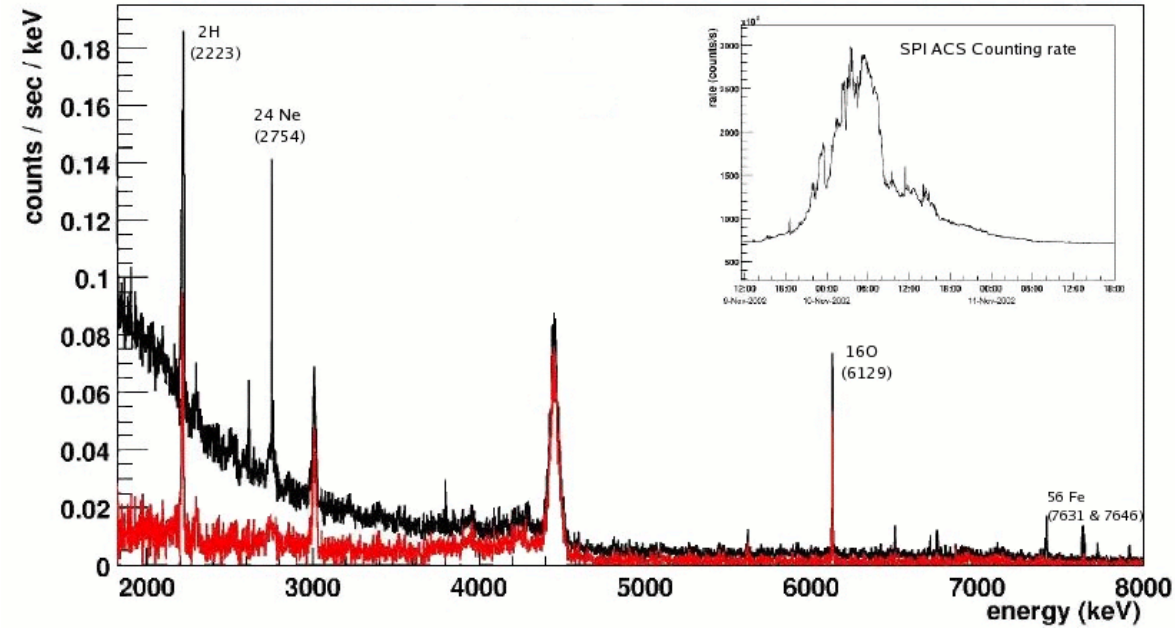

Figure 10 - SPI GeD spectrum obtained during a solar flare, probing the instrument ability to resolve lines in the MeV energy range. The black curve shows the total counts measured. The red one is the background-subtracted spectrum. SPI ACS light curve during the solar flare is also shown on the top right corner.

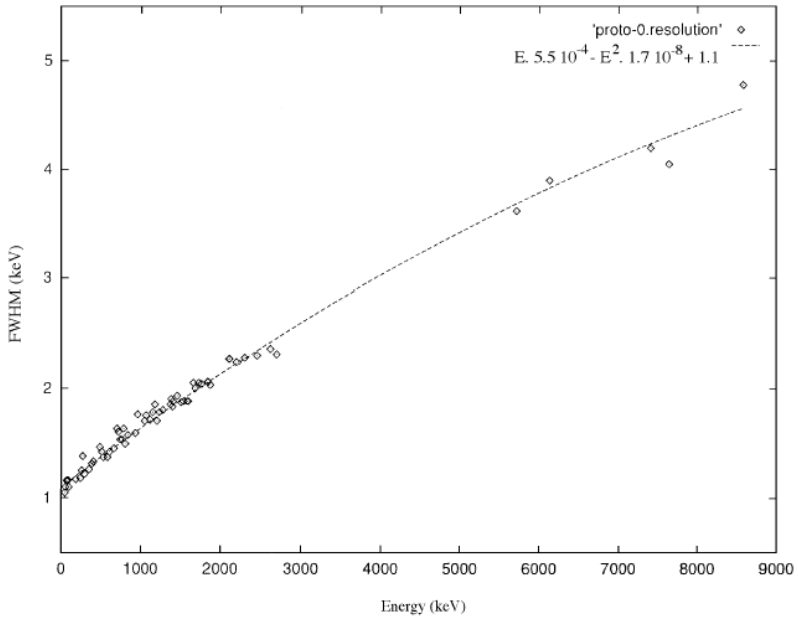

Figure 11 - Energy resolution of an individual SPI detector, measured while using laboratory detectors. The resolution of the full instrument with all the 17 detectors is slightly lower than this.

Table 2 - Energy resolution (FWHM), continuum and narrow-line sensitivities of SPI (3σ detection in 10^6 sec). Note that the line sensitivities is a function of the energy close to the lines and can vary strongly with it. The continuum sensitivities are for ΔE=E/2. Corrections for failures of detector elements, source aspect angle and dithering must be applied (see Sections 4.2.4, 4.2.5 and 4.2.6).

Energy (keV)	Resolution (keV)	Continuum sensitivity (ph cm^{-2} s^{-1} keV^{-1})	Line sensitivity (ph cm^{-2} s^{-1})
50	1.53	9.2×10^{-6}	5.6×10^{-5}
100	1.56	3.3×10^{-6}	3.3×10^{-5}
500	1.93	1.2×10^{-6}	2.3×10^{-5}
1000	2.21	8.8×10^{-7}	2.4×10^{-5}
5000	3.62	1.4×10^{-7}	1.1×10^{-5}

The energy resolution of the GeDs evolves with time, and a continuous monitoring of the resolution is needed to analyse properly the data from SPI. This is because the GeD performance degrades with the damages created within the crystal by incident radiation (mainly protons and neutrons). This increases the number of hole traps within the active detection volume. In space, the particle flux is high enough to produce substantial degradation of the GeDs over times of a

few months (about 20% in 6 months). The damage is not permanent and can be corrected by the annealing procedure.

4.2.3 Annealing

The annealing process consists in heating the GeDs in order to restore the quality of the crystalline lattice and suppress the trapping sites. The success of the process strongly depends on the initial damage, on the annealing temperature and on the duration of the annealing cycle (it was found that about 100 hours of annealing were necessary to restore the full resolution close to pre-launch values). The first SPI annealing cycle was performed on February 2003. Since then, twelve annealings have been carried out, all of which increased the energy resolution as expected. Figure 12 shows the mean energy resolution of the camera at 1764.3 keV as a function of time. The recovery of the energy resolution after each annealing cycle is of the order of 10-20%.

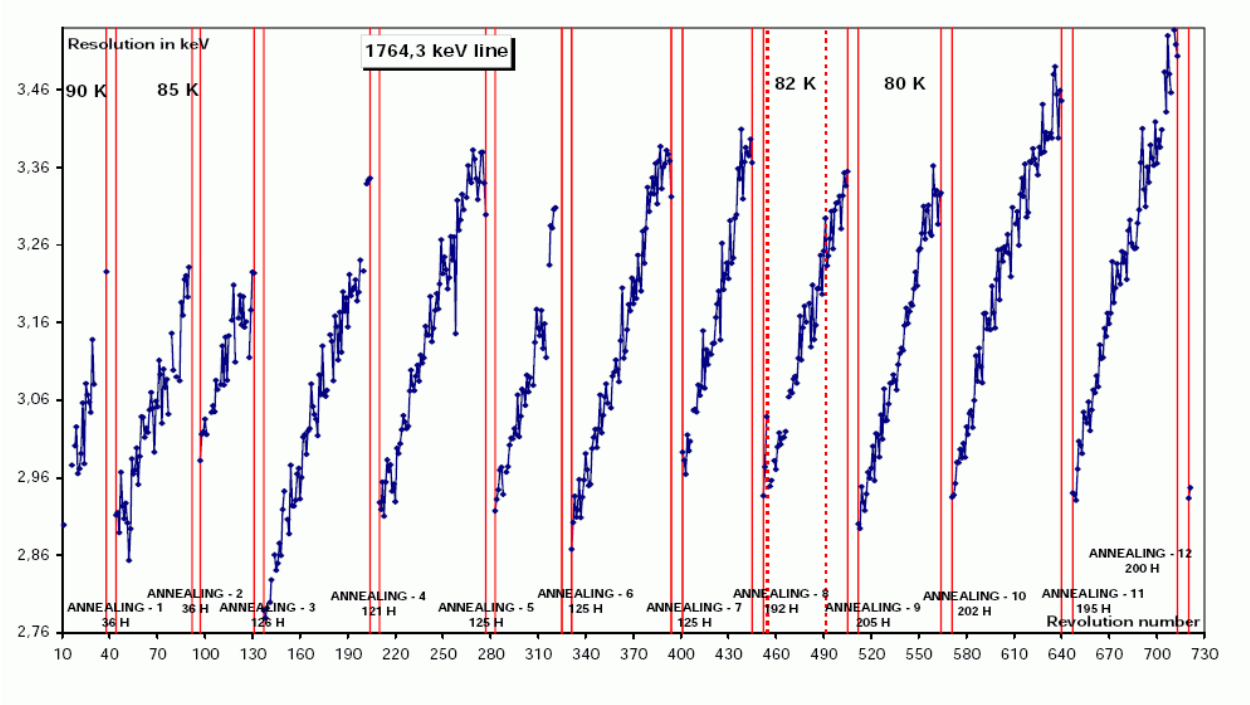

Figure 13 - The evolution of energy resolution at 1764.3 keV as a function of time in between the annealing periods (from the SPI team).

4.2.4 Sensitivities

The instrument performance numbers (energy resolution, continuum and line sensitivities) at specific energies are shown in Table 2. The sensitivities provided in this table correspond to 3σ detections in 10^6 seconds of pure integration time. The quoted sensitivities only include the statistical errors, the impact of imaging algorithm and background subtraction methods are not included. The line sensitivities indicated are for narrow lines. The continuum sensitivities are for $\Delta E=E$, and are calculated from the narrow line sensitivity by dividing those by $\sqrt{R \cdot \Delta E}$, where R is the instrument resolution for lines. The sensitivity limit is 5×10^{-5} ph cm^{-2} s^{-1} at 511 keV, and

2.5×10^{-5} ph $cm^{-2} s^{-1}$ at 1809 keV. The continuum and line sensitivities of SPI are displayed in Figure 10 and Figure 11, respectively. Users should also be aware that the 511 sensitivity is worse than the surrounding continuum, due to the strong 511 keV background line originating in the instrument.

Note that the failure of detectors #2 and #17 implies loss of single events from these detector units, and increased single-event rates in neighbouring detectors from the former multiple-events of #2 and #17 (scattering into neighbouring detectors). The sensitivity loss thus depends on event type selection, and corresponds to between 5% for continuum and 20% for low-energy lines. The sensitivity Figures (10 and 11) are for the 19-element Ge camera, hence they do not include these effects.

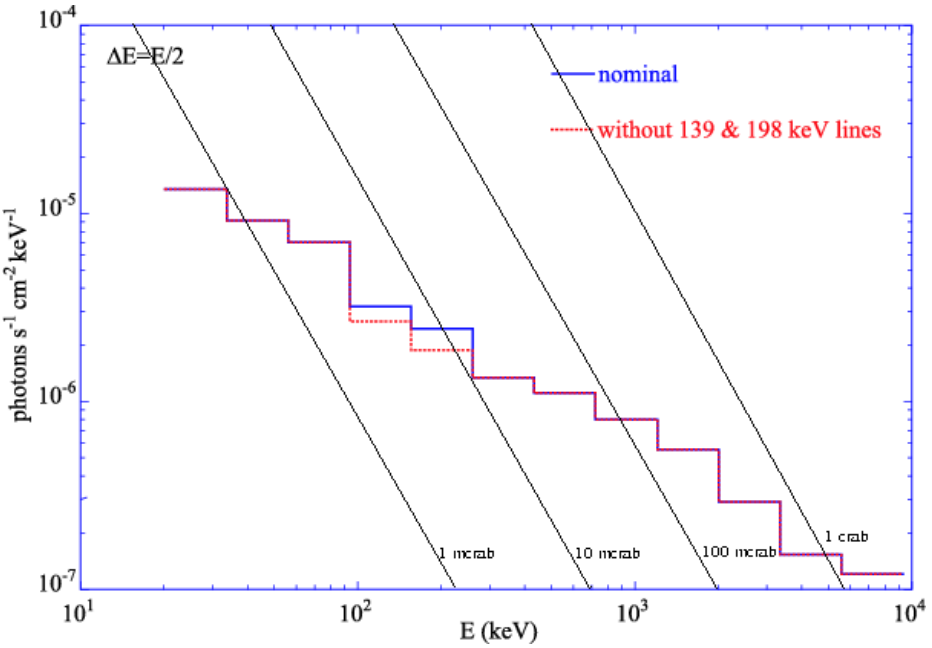

Figure 14 - The continuum sensitivity of SPI for an on-axis, 3σ detection in 10^6 seconds. Fluxes are for E=E/2. The dashed lines indicate extrapolation from X-rays using a power law with a photon index equal to -2.1 for 1, 10 and 100 mCrab. Corrections for failures of detector elements, source aspect angle and dithering must be applied when necessary (see Sect. 4.2.5, 4.2.6 and Roques et al., 2003, A&A vol. 411, L113.)

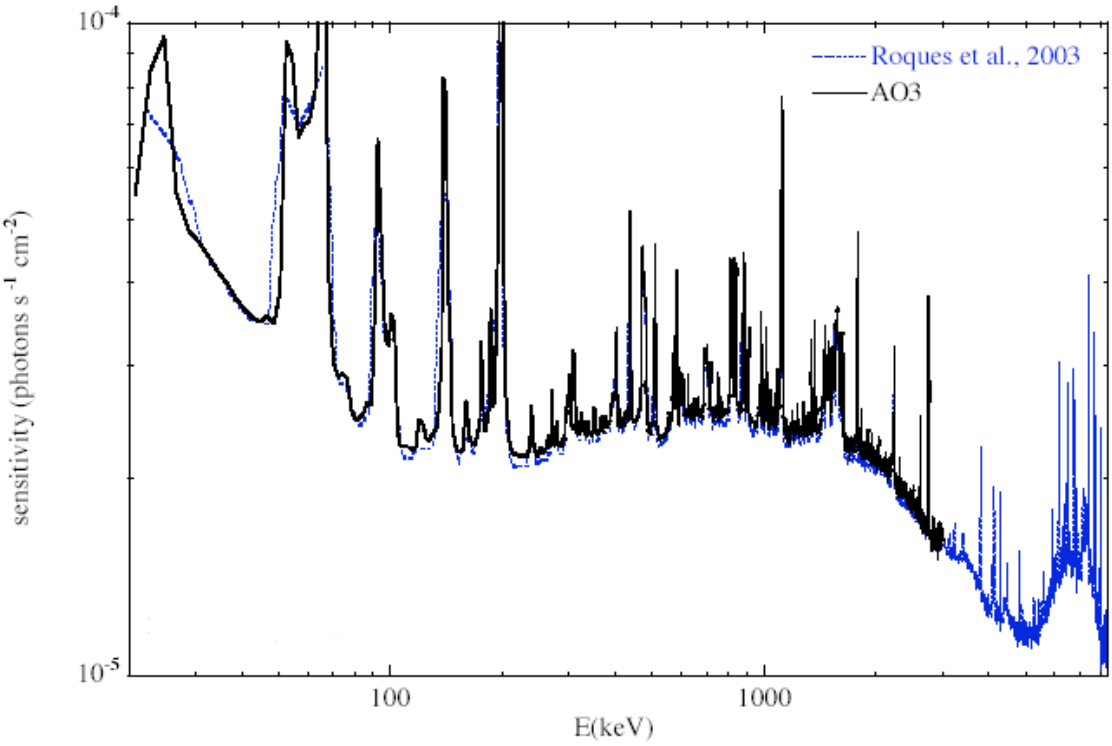

Figure 15 - The SPI 3σ narrow-line statistical sensitivity (w.r.t. the instrument resolution) for an on-axis point source. Data is the combination of SE and ME2 events. Integration time is 10^6 seconds for each data set. Live times are 88% for Roques et al. 2003 (A&A vol. 411, L113) and 86% for AO3 data. Corrections for failures of detector elements, source aspect angle and dithering must be applied when necessary (see Sect. 4.2.5 and 4.2.6). From J.-P. Roques.

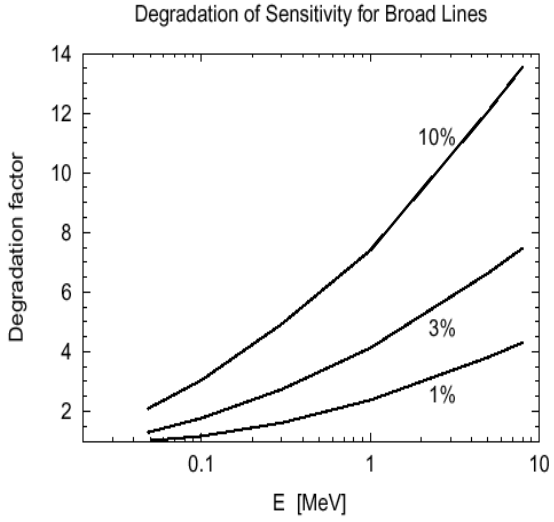

Figure 16 - The degradation factor or the line sensitivity for broad lines (with a width of 1, 3 and 10 % of the line energy) as a function of energy.

4.2.5 Dithering sensitivity degradation

Although dithering is essential for the identification and removal of the SPI background, it has the disadvantage that the source is not observed for the full integration time in the centre of the fully coded field of view. The SPI response falls off towards the edge of the field of view, and therefore dithering degrades the sensitivity of the instrument. The above quoted sensitivities are derived for a source on axis, and do not take into account dithering. When using a 5x5 dither pattern, the sensitivity is degraded by a factor of 0.8374 (i.e., the sensitivities given in Table 2 should be divided by this number to get the effective sensitivity).

Table 3 - Sensitivity degradation factor as a function of the off-axis distance, for hexagonal and 5 by 5 dither patterns.

Off axis distance (deg)	Sensitivity degradation	
	Hex	5 x 5
0	1.0	0.8374
1	0.6655	0.7925
2	0.7638	0.8004
3	0.6838	0.7879
4	0.7147	0.7874
5	0.7056	0.7746
7.5	0.6309	0.7357
10	0.5505	0.6718
12.5	0.4938	0.5918
15	0.3749	0.5002
17.5	0.1888	0.3774
20	0.0886	0.2047
25	0.0	0.0148
30	0.0	0.0

4.2.6 Detection of off-axis sources

The wide field of view of SPI allows the detection of off-axis sources. However, the SPI sensitivity varies with the incidence angle, and corrections should be applied accordingly. Any source extraction at the edge of the field of view requires careful analysis.

Details on the sensitivity degradation factor as a function of the off-axis distance for the hexagonal and 5x5 patterns are provided in Table 3.

4.2.7 Timing capabilities

In the standard photon by photon mode, each photon data set includes timing information given by a 102.4 μs clock signal. This clock is synchronised to the on-board clock, and thus to the U.T.C. There are, however small uncertainties affecting the event time accuracy, namely:

- the accuracy of the on-board clock and the synchronisation;
- the conversion between on-board time and U.T.C.;
- the conversion between U.T.C. arrival time at the spacecraft and the arrival time at the solar system barycentre.

The resulting SPI timing resolution is 129 μs (3σ accuracy) with a 90% confidence accuracy of 94 μs. Timing analysis of the Crab data has revealed that the absolute timing accuracy is about 40 μs (1σ uncertainty; see Kuiper et al., 2003, A&A, vol 411, L31).

The pulse profile of the Crab pulsar, as measured by SPI, is shown Figure 12: this illustrates the capabilities of the instrument performing timing analysis.

Note that due to strict limits on the telemetry allocation, the SPI instrument was operated during a large part of AO1 in a mode where the single event photons were only down-loaded as part of the histograms, severely degrading the time resolution for these events to 30 minutes. The increased telemetry budget for SPI allowed to restore the original time resolution for single events. Therefore, in combining new observations with data from the 2002-early 2003 period, proper operation mode data must be selected.

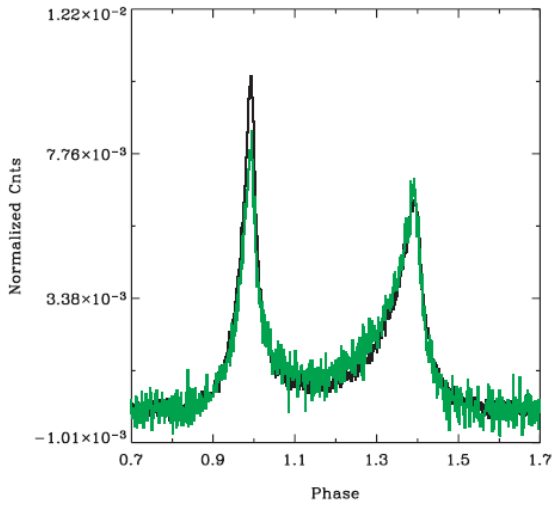

Figure 17 - Phase histogram of the Crab pulsar (PSR B0531+21; P=33 ms) as measured by SPI (20-50 keV, green). The pulse profile as measured by RXTE/PCA (2-30 keV, black), during nearly simultaneous observations, and produced with the same ephemeris, is shown for comparison. (Kuiper et al., 2003, A&A vol. 411, L31).

4.3 Instrumental characterisation and calibration

The SPI instrument was tested and calibrated with radioactive sources on ground, before the launch. Further testing was performed during the Performance and Verification (PV) phase of the mission, and has been carried out thereafter by conducting regular calibration observations. The sensitivities, resolution, and other characteristics given in this document represent the current best knowledge of the SPI instrumental characterisation.

Observations of the Crab nebula and pulsar are carried out regularly to verify the calibration status of the instrument. Up to one revolution during each visibility period of the field, i.e., twice per year, is devoted to these observations. This allows measuring the instrument imaging and spectroscopic performance, the background characteristics, the instrument sensitivity and the off-axis response, providing the calibration that will be used for data processing. Figure 18 shows the Crab spectrum as measured by SPI.

Crab calibration observations are also used to study and improve the cross calibration between the INTEGRAL instruments. There are now very little systematic differences in the residuals from one Crab observation to the other and a very good match between IBIS/ISGRI and SPI. For further details in the status of the IBIS/SPI cross calibration we refer the reader to the ISDC Astrophysics Newsletter, #21, and the INTEGRAL "*Mission overview, policies and procedures* document".

Instrumental background lines are also used to calibrate the instrument. Being originated in the instrument itself, instrumental lines are not expected to be intrinsically broadened or shifted due to the Doppler effect. Lines originating in the BGO shield (e.g. 511 keV, 6.1 MeV O line) are currently used for energy calibration, whereas the lines that originate from materials inside the cryostat (and have known intensities) can be used to measure the Ge detector efficiency. These calibrations are carried out once per revolution and per detector.

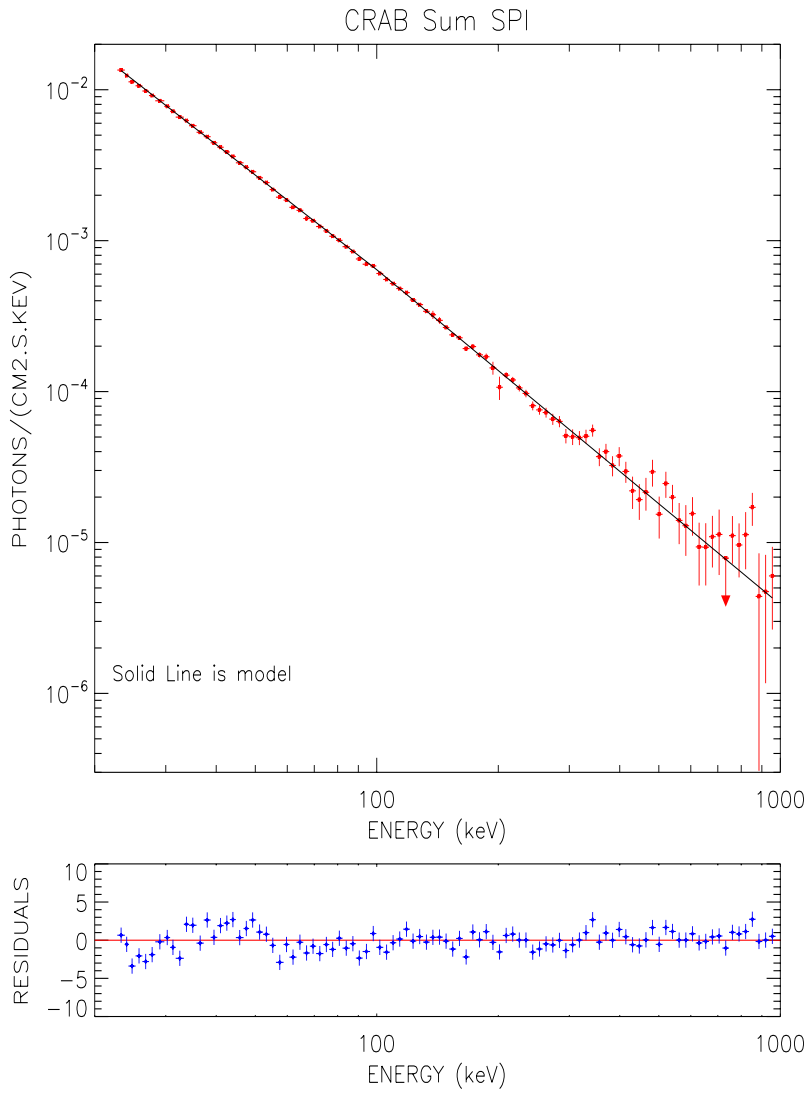

Figure 19 - Best-fit of the Crab SPI photon spectrum, which is the sum of all data available in the same configuration (with 17 detectors, i.e., after revolution 214, and with a 5x5 dither pattern). This leads to 326 ks exposure, distributed over 7 revolutions. The spectrum has been extracted using the arf and rmf matrices delivered in OSA 7. The fit to the data is done with a broken power-law model (break energy 100 keV), with photon indexes of 2.08 and 2.22 (Γ_ν^2=1.75 for 97 d.o.f. and 0% systematics). The flux at 100 keV is 6.44x10^{-4} ph cm^{-2} s^{-1}. (Jourdain and Roques 2008, to appear in Proceedings of the 7th INTEGRAL Workshop).

The detector gains, thresholds and resolution versus energy are determined from normal event data and ACS off spectra (for consistency checks) in the routine monitoring task of ISDC. Finally, after every detector annealing, a thorough check of the instrument imaging and spectroscopic response is done, since these may change as a result of the annealing process.

4.4 Astronomical considerations on the use of the instrument

The SPI instrument is designed as a spectrometer; therefore it should primarily be used for high-resolution spectroscopy on sources with (narrow) lines, possibly on top of a continuum. Given the imaging qualities of the instrument, it can also be used for wide field imaging of diffuse emission, especially in (narrow) emission lines. However, if high resolution imaging, observations of sources with only continuum emission, or very broad lines are needed, the IBIS instrument might be better suited as a prime instrument, at least below a few hundred keVs.

The prime astrophysical topics to be addressed with SPI are: nucleosynthesis processes, supernova theories, nova theories, interstellar physics and pair plasma physics in compact objects (neutron stars, black holes). A number of interesting astrophysical lines fall in the SPI energy range, some of them are complied in Table 4.

Table 4 - Some gamma-ray lines from cosmic radioactivity in the SPI energy range.

Isotope	decay chain	line energies (MeV)	Mean life (year)
e^+	$E^+ + e^-$ photon	0.511	~$1x10^5$
^{56}Co	(^{56}Ni) ^{56}Co ^{56}Fe	0.847, 1.238	0.31
^{22}Na	^{22}Na ^{22}Ne	1.275	3.8
^{44}Ti	^{44}Ti ^{44}Sc ^{44}Ca	1.156	89
^{26}Al	^{26}Al ^{26}Mg	1.809	$1.0x10^6$
^{60}Fe	^{60}Fe ^{60}Co ^{60}Ni	1.173,1.322	$2.2x10^6$

We now present a summary of some results obtained with SPI to illustrate its capabilities (the selection is by no means exhaustive).

Thanks to its large field of view, and to the dithering strategy, SPI is optimum for imaging large sky areas, through the combination of a large set of individual pointing. This allows (for example) generating maps of diffuse continuum and line emission in the Galaxy (see Figure 14, Figure 15). The continuum images of the Galaxy reveal the transition from a point source dominated hard X-ray sky to a diffuse emission dominated soft gamma-ray sky (Figure 14; see, for example, Bouchet et al., 2008, ApJ 679, 1315, and references therein). Apart from its suitability in the study of diffuse emission, the spectrometer SPI has also proved its superb capabilities in the study of point-like emission in the hard X-ray and soft gamma-ray regime. The SPI all-sky survey analysis, based on 4 years of SPI observations (~51 Msec), has also provided a complete catalogue of 173, 79, 30, and 12 sources detected above ~3.5 σ in the 25-50 and 50-100 keV bands and above ~2.5 σ in the 100-200 and 200-600 keV bands (Bouchet et al., 2008, ApJ 679, 1315). All but one are associated (within 1°) with at least one IBIS source (Bird et al. 2007, ApJS, 170, 175). Above 600 keV, only the Crab Nebula, Cyg X-1, GRS 1915+105, and GRS 1758-258 are detected, with the former two still emitting above 2 MeV.

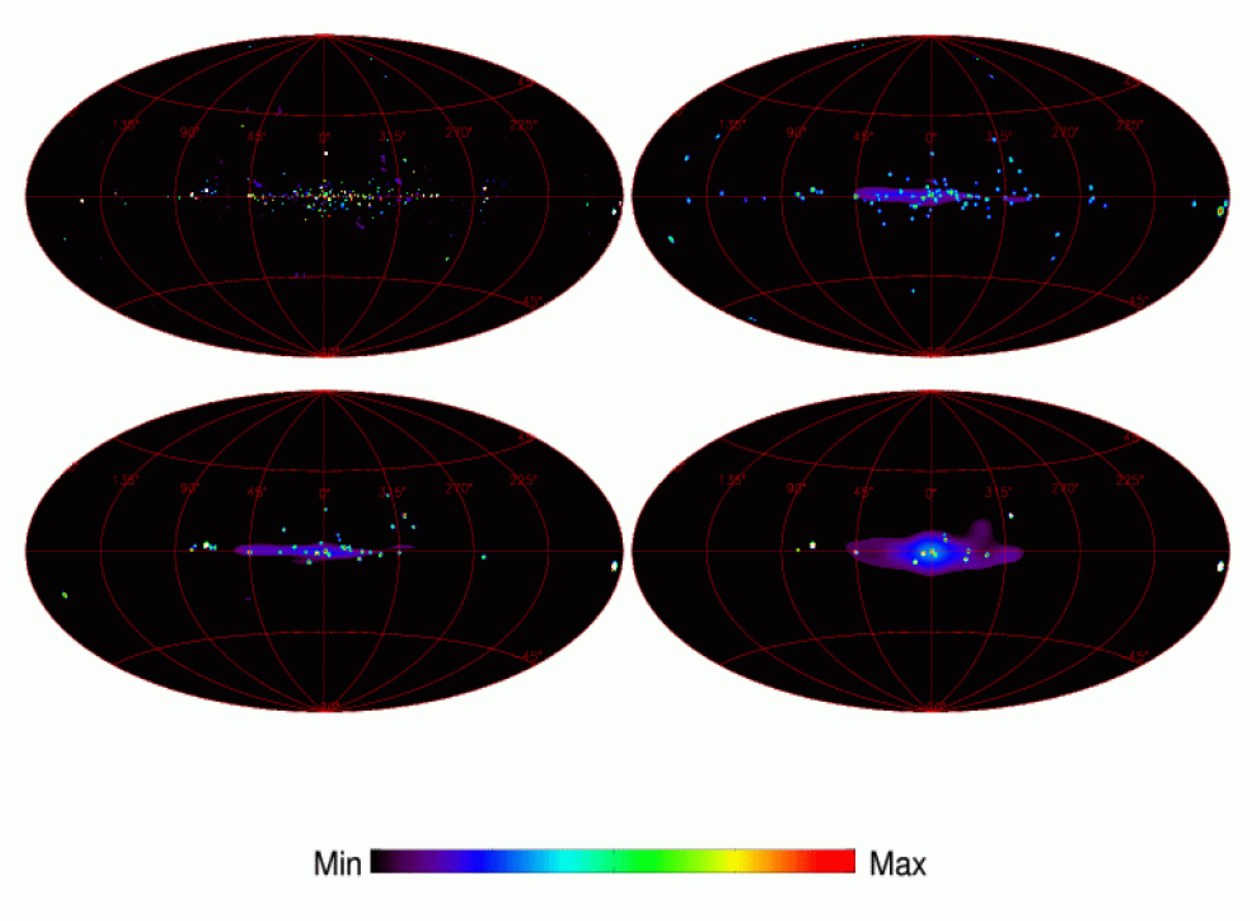

Figure 20 – SPI sky maps in the 25-50 keV (top, left), 50-100 keV (top, right), 100-200 keV (bottom, left) and 200-600 keV (bottom, right) energy bands. At low energy, the sky emission is dominated by sources, while a "diffuse/extended" structure appears above 200-300 keV, in a domain corresponding to the annihilation radiation. The color scale is logarithmic, and the scale is saturated to reveal the weakest sources. These images have been obtained by maximum-likelihood fitting of point sources from a reference catalogue, plus diffuse-emission models represented from a set of pixons (16x2.6 deg in size). From Bouchet et al., 2008, ApJ 679, 1315).

The study, with SPI, of the spatial distribution of the positron annihilation emission line in our Galaxy, and of its energy spectrum, has provided unprecedented results. For the first time, the SPI sky maps of the 511 keV line and the positronium continuum revealed that the diffuse 511 keV emission is located towards the Galactic Centre only (Knödlseder et al., 2005, A&A vol. 441, L513). Deeper maps of the Galaxy have recently revealed an asymmetry in spatial distribution of the 511 keV line emission coming from the inner Galactic disk (~10-50° from the Galactic Centre). This asymmetry resembles the (asymmetric) spatial distribution of the hard low mass X-ray binaries (LMXBs) in the inner Galactic disk, indicating that they may be the dominant origin of the positrons (Figure 21; see Weidenspointner et al., 2008, Nature, vol 451, Issue 7175, L159).

Furthermore, the superb energy resolution of SPI has allowed detailed spectral modelling of the annihilation emission in the 400-600 keV range. Three components of the line emission have been observed: a narrow (2 keV) line at 511 keV, a broad (5 keV) component, and a continuum emission due to the decay of ortho-positronium at energies below 511 keV (Figure 16; see Jean et al., 2006, A&A vol. 445, L579 for further details).

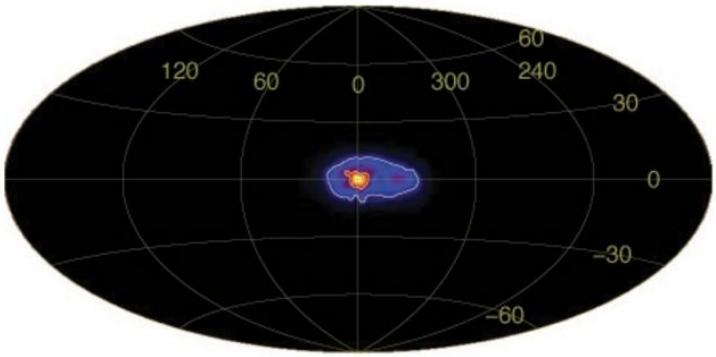

Figure 22 - Combining more than 4 years of observations, the SPI 511 keV positron annihilation line image from the inner Galaxy shows a bright main component centered on the Galaxy's center with an extent of about 8 deg (FWHM) and an indication of the annihilation emission from the disk of the Galaxy. The latter even appears asymmetric with enhanced brightness in the fourth quadrant. From Weidenspointner et al., 2008, Nature, Vol 451, Issue 7175, L159.

SPI images in the 1809 keV gamma-ray line from ^{26}Al have confirmed the basic emission features established by COMPTEL: a strong Galactic ridge emission from the inner Galaxy, and a prominent feature in Cygnus (see, for example, Knödlseder et al., 2007, ESA Conf.Proc. SP-622, 13, and references therein). Furthermore, deep observations of the Galactic Plane (~4 Msec) have revealed that the emission from the longitude range 10 to 40 is red-shifted by about 0.2 keV, while emission from longitude range -10 to -40 is blue-shifted by about 0.4 keV with respect to the 1809 keV emission observed from the Galactic Centre (Figure 24; for further details see Diehl et al., 2006, Nature, vol. 439, Issue 7072, L45).

^{60}Fe decay gamma-ray lines 1173 keV and 1333 keV have also been measured by SPI. Almost three years of data have provided a ^{60}Fe signal from the Galaxy

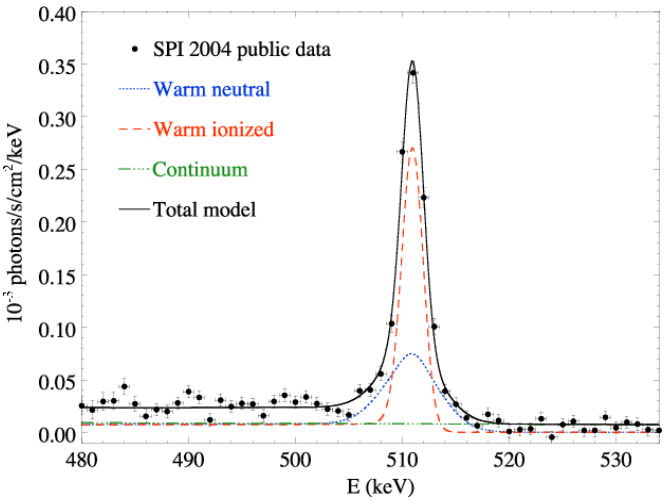

Figure 23 - Spectrum of the electron-positron 511 keV annihilation emission, showing the narrow and broad line components and the continuum emission below 511 keV due to the decay of ortho-positronium. (Jean et al., 2006, A&A, vol. 445, L579).

with a significance of 4.9 σ. With the same method and data, the ratio of ^{60}Fe to ^{26}Al was derived to be ~ 15%, a value consistent with current theoretical models (Wang et al., 2007, A&A, vol. 469, L1005). ^{60}Fe emission from the Cygnus and Vela regions has not been found up to now.

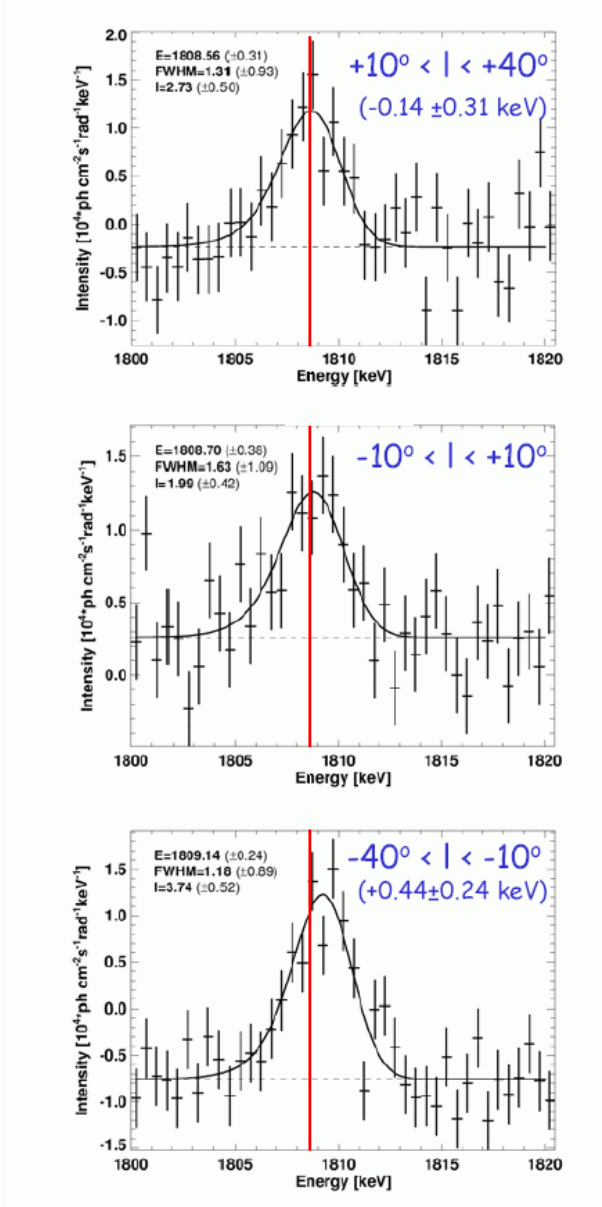

Figure 25 - The ^{26}Al line profiles obtained at different galactic locations. A clear shift in the line centroid energy in the top and bottom panels, compared to the center one, is visible. The shift is fully consistent with the Doppler shift of the line energy (1809 keV) expected from galactic rotation. The observed line shift is less than 0.5 keV, demonstrating the superb quality of SPI's spectral resolution. (From Diehl et al., 2006, Nature, vol. 439, Issue 7072, L45).

5 Observation "Cook book"

5.1 How to estimate observing times

The formal way to calculate accurate observing time is via the Observing Time Estimator (OTE), which can be found at: http://integral.esac.esa.int. However, in this section we provide an easy way for observers to estimate the observing times using simple formulae. The times calculated in this way are reasonably accurate, and are for most cases within a few percent from the OTE calculated times. In the worked examples we show both estimations for comparisons. Note, however, that ISOC will only use the OTE to assess the technical feasibility of the proposals. General observers can request observations of a gamma-ray line (flux expressed as ph cm^{-2} s^{-1}), or observations of the integrated continuum flux over a certain energy band (flux also expressed in ph cm^{-2} s^{-1}). Examples of both instances are presented in the following examples.

Note: the observers should make sure that observing times entered into PGT allow the completion of at least one full dither pattern (i.e., minimum of 12600 seconds for an hexagonal dither and 45000 seconds for a 5 x 5 dither).

5.1.1 Gamma-ray line

The observation time, T_{obs} (in kiloseconds), is estimated using the relation:

$$T_{obs} = 1 \cdot 10^3 \cdot \left(\frac{N_\sigma}{3} \cdot \frac{S_{line}}{F_{line} \cdot F_{rac}} \right)^2 \cdot \frac{\Delta E}{R} \cdot \frac{1}{1 - f_{dead}},$$

where:

- N_σ is the sigma required in the detection;

- S_{line} is the 3σ, on-axis point source, SPI narrow line sensitivity at the considered energy, for 10^6 s integration time and a lifetime of 100%. The values of this parameter are shown in Table 2;

- F_{line} is the source line flux in ph cm^{-2} s^{-1};

- F_{rac} is the sensitivity degradation factor due to dithering, or to the source being off-axis. See Table 3, Sections 4.2.5 and 4.2.6 for details;

– ΔE is the expected width of the gamma-ray line (FWHM in keV);

- R is the energy resolution of the spectrometer (in keV). It depends on the energy. The values of this parameter are given in Table 2;

- f_{dead} is the fraction of dead-time (15%). This parameter is described in Section 3.3.

5.1.2 Gamma-ray continuum

The observation time, T_{obs} (in kiloseconds), is estimated using the relation:

$$T_{obs} = 1 \cdot 10^3 \cdot \left(\frac{N_\sigma}{3} \cdot \frac{S_{line}}{F_{line} \cdot F_{rac}} \right)^2 \cdot \frac{\Delta E}{1.5R} \cdot \frac{1}{1 - f_{dead}}$$

$$= 1 \cdot 10^3 \cdot \left(\frac{N_\sigma}{3} \cdot \frac{S_{cont}}{F_{cont} \cdot F_{rac}} \right)^2 \cdot \frac{E}{2\Delta E} \cdot \frac{1}{1 - f_{dead}},$$

where:

– F_{int} is the flux integrated over the specified band (in ph cm^{-2} s^{-1});

– F_{cont} is the continuum flux in the specified band (in ph cm^{-2} s^{-1} keV^{-1});

– ΔE is the width of the energy band corresponding to the specified flux (in keV);

– S_{cont} is the continuum sensitivity as given in Table 2. The continuum sensitivity can be calculated from the line sensitivity, using:

$$S_{cont} = S_{line} / \sqrt{1.5R\Delta E}$$

All other parameters are as described above. The factor 1.5 is used to correct the gamma-ray line sensitivity, which is calculated assuming that the total counts in a line are contained in an energy band of 1.5 times the spectral resolution (FWHM). Actually, 1.5 times the resolution contains ~95% of the line counts.

In previous versions of the OTE, the band over which the flux is specified should not be too broad (maximum ΔE=E/2) since the sensitivities were for ΔE=E/2. However, with the latest versions of the OTE, observers can specify a power-law slope and then the OTE will split the total energy band up into many small bands, and combine all the results.

5.2 Worked examples

In this section we present some examples of observations with SPI for which we calculated the observing times with the formulae given above, and the OTE. Note that for lines, the exposure time derived from the OTE differs from the one calculated from the formula. This is because the OTE uses sensitivities at a much higher energy resolution than tabulated in Table 2 (see Figure 7). The examples below (for lines) are therefore only intended as an order of magnitude estimate; one should use the exposure times obtained with the OTE.

Example 1a: the ^{26}Al line at 1809 keV, with a width of 3 keV (FWHM), and an integrated flux of 5x10^{-5} ph cm^{-2} s^{-1}, to be observed with a 5x5 dither pattern. The requested significance is 3σ. The sensitivity at this energy is 2.1x10^{-5} ph cm^{-2} s^{-1}, the resolution is 2.553 keV, and the sensitivity degradation factor for the 5x5 dither pattern is 0.8374. Using these numbers, the required observing time would be 224 ksec, or 2.59 days (the OTE gives 493 ksec).

Example 1b, to show the correspondence between the manual and the OTE results at an energy where the line sensitivity is fairly constant: a line at 2000 keV, with a 3 keV width, and a integrated line flux of $5x10^{-5}$ ph cm^{-2} s^{-1}, observed with a 5x5 dither pattern. The requested significance is 3σ. The sensitivity at this energy is $2.0x10^{-5}$ ph cm^{-2} s^{-1}, the resolution is 2.634 keV, and the sensitivity degradation factor for the 5x5 dither is, again, 0.8374. With these numbers, the required observing time would be 295 ksec, or 3.41 days (the OTE gives 337 ksec).

Example 2: the same 1809 keV line, but now observed with an hexagonal dither (sensitivity degradation factor of 1.0) for a significance of 3σ would require 157 ksec, or 1.82 days (however, keep in mind that this mode is only applicable for isolated point sources; the OTE gives 346 ksec).

Example 3: a continuum band of 150 keV width, centred at 350 keV, with a continuum flux of $2x10^{-5}$ ph cm^{-2} s^{-1} keV^{-1}, observed with a 5x5 dither for a significance of 10σ. The continuum sensitivity for this energy is $1.4x10^{-6}$ ph cm^{-2} s^{-1} keV^{-1}, the resolution is 1.80 keV, and the sensitivity degradation factor is again 0.8374. This observation would then require 103 ksec, or 1.19 days (the OTE gives 102 ksec with an in-band flux of $3.0x10^{-3}$ ph cm^{-2} s^{-1}).

Example 4: the ^{44}Ti line at 1.160 MeV in a supernova remnant (e.g., Cas A). The line width is 2000 km s^{-1} (or 7.73 keV), the integrated line flux $1x10^{-4}$ ph cm^{-2} s^{-1}. The source should be observed with a 5x5 dither, for a significance of 5σ. The sensitivity of the instrument at this energy is $2.4x10^{-5}$ ph cm^{-2} s^{-1}, the resolution is 2.28 keV, and the sensitivity degradation factor is again 0.8374. The required observing time would then be 586 ksec or 6.78 days (the OTE gives 861 ksec).

Example 5: a broad, red-shifted 511 keV line. The energy of the line is 470 keV, with a width of 5000 km s^{-1} (or 16 keV), and an integrated line flux of $3.3x10^{-4}$ ph cm^{-2} s^{-1}. The observation is to be performed using the hexagonal dithering mode (isolated source), for a significance of 5σ. The sensitivity of the instrument at this energy is $4.6\ 10^{-5}$ ph cm^{-2} s^{-1}, the energy resolution is 1.93 keV and the sensitivity degradation factor is 1.0. This observation would then need 347 ksec, or 4.02 days (the OTE gives 274 ksec).

Example 6: a continuum band of 500 keV width, centred at 4 MeV, with a continuum flux of $1x10^{-6}$ ph cm^{-2} s^{-1} keV^{-1}. The observation should use a 5x5 dither pattern, and requires a 3σ detection. The sensitivity of the instrument at this energy is $1.4x10^{-7}$ ph cm^{-2} s^{-1} keV^{-1}, the resolution is 3.32 keV and the sensitivity degradation factor is 0.8374. This observation would require 172 ksec, or 2.0 days (the OTE gives 698 ksec, assuming a constant photon flux over the energy band, given a flux of $5x10^{-4}$ ph $cm^{-2}s^{-1}$ in this band).

Example 7: an extended source with a size of 4.8 arcminutes and a continuum flux of $2x10^{-5}$ ph cm^{-2} s^{-1} keV^{-1} in a band of 150 keV, centered at 350 keV. With an angular resolution of 2.5 degrees, the source can be resolved in $(4.8/2.5)^2$ pixels. In 102 ks, a sensitivity of 10/(4.8/2.5) (see example 3), or 5.2σ, can be reached.